Jour. Korean Inst. Mining Geol.
V. 17, No. 2, 1984, p. 115-139

Reflectance and Microhardness Characteristics of Sulfide Minerals from the Sambong Copper Mine

Se Jung Chi*

Abstract : The Cu-Pb-Zn-Ag hydrothermal vein-type deposits which comprise the Sambong mine occur within calc-alkaline volcanics of the Cretaceous Gyeongsang Basin. The ore mineralization took place through three distinct stages of quartz (I and II stages) and calcite veins (III stage) which fill the pre-existing fault breccia zones. These stages were separated in time by tectonic fracturing and brecciation events.

The reflection variations of one mineral depending on mineralization sequence are considered to be resulted from variation in its chemical composition due to different physico-chemical conditions in the hydrothermal system. The reflection power of sphalerite increases with the content of Fe substituted for Zn. Reflectances of the sphalerite grain are lower on (111) than on (100) surface. The spectral profiles depend on the internal reflection color. Sphalerite, showing green, yellow and reddish brown internal reflection, have the highest reflection power at 544mμ (green), 593mμ (yellow) and 615mμ (red) wavelength, respectively. Chalcopyrite is recognized as biaxial negative from the reflectivity data of randomly oriented grains measured at the most sensitivity at 544mμ.

The microindentation hardness against the Fe content (wt. %) for the sphalerite increases to 8.05% Fe and then decreases toward 9.5% Fe content. Vickers hardness of the sphalerite is considerably higher on surface of (100) than on (111). The relationship between Vickers hardness and crystal orientation of the galena was determined to be $VHN_{(111)} > VHN_{(210)} > VHN_{(100)}$. The softer sulfides have the wider variation of the diagonal length in the indentation. Diagonal length in the indentation is pyrite< sphalerite<chalcopyrite<galena. Each ore mineral studied produce characteristic indentation shape and fracture, depending on its crystal orientation.

INTRODUCTION

The Cu-Pb-Zn-Ag hydrothermal vein-type deposit (Sambong mine) occurs within calc-alkaline volcanics of the Cretaceous Gyeongsang Basin. The major ore mineral, chalcopyrite, together with minor amounts of galena, sphalerite, and pyrite is contained within fissure-filling hydrothermal quartz veins. The gangue minerals consist mainly of quartz and small amounts of calcite, chlorite, and sericite. The average ore grades of the Sambong mine are 1.89wt.% Cu, 186g/metric ton Ag(5.98 troy oz/ton), and 0.94g/metric ton Au (0.03 troy oz/ton). The total ore reserves of the Sambong mine are estimated 38,075 metric tons. A few copper deposists in Gyeongsang Basin were studied previously by park (1983).

The aims of the present study were to document the reflectivity-microhardness characteristics of the ore minerals. The correlation between the physical properties of the ore minerals were illustrated and their dependence on the paragenetic sequence, composition and crystal orientation were determined.

GEOLOGY

The Sambong mine studied exist in the southwestern part of the Yuchon Group within the Gyeongsang Basin. The geology of this mining area consists of, in ascending order, the Goseong Formation, and andesites and andesitic tuffaceous

*Department of Geology, Korea University

rocks.

The Goseong Formation consists of, in ascending order, green tuffaceous conglomerate, fine-to medium grained greenish gray tuffaceous sandstone, and reddish tuffaceous shale. Thin beds of greenish tuff are found interbedded in upper parts of this formation. Tuffaceous conglomerates do not occur in the mining area. Porphyritic and grayish black vitric andesites occur as extrusive rocks overlying the Goseong Formation (Chang, etc., 1983), or in places as dikes in the mining area. The porphyritic andesites have plagioclase phenocrysts displaying a characteristic seriated texture.

Andesitic tuffaceous rocks conformably overlie the Goseong Formation and in some places overlie andesites in the mining area. These rocks consist of two major rock types. The lower parts are characterized by dark greenish to greenish gray lapilli tuff and the upper parts by dark gray welded tuff. The size of rock fragments in lapilli tuff ranges from 2 to 6cm in length and increases with depth. The welded tuff are composed of mainly feldspar fragments, which strongly altered to sericite, and glass shards.

In the mining area, an extensive system of parallel fractures in volcanic rocks and tuffaceous sedimentary rocks has been mineralized over a horizontal distance of 1.5km. Only the Sambong mine in this area is currently being worked economically.

The pre-existing fracture systems are mainly fault breccia zones. The quartz veins that fill this fracture system are narrow and only rarely exceed 2.5m in width. The veins strike N–S to N13°W. The dips of the veins from two groups, one group dipping 65° to 85°w, and the other 50° to 70°E. Brecciated fragments (less than 30cm long) of the wall rock are often contained, forming chambered veins where the vein thickness increases.

The quartz veins are tabular and are filled dominantly with white quartz. Surface outcrops of the veins tend to be sulfide-poor, but at depth the quartz veins contain disseminated sulfides with occassional concentration of ore sulfides. Certain regions of the vein are richer and give rise to definable ore-shoots. These veins are accompanied in the upper parts of the ore-shoots by relatively larger concentrations of galena and sphalerite, so that some veins are worked for these Pb-Zn minerals. The ore vein dips 60° to 70°W at the ground surface, 50° to 55° W at 124m above sea level and 60° to 65° W at 94m above sea level. This type of vertical bending controls the localization of the richest concentrations of the ore (So and Chi, 1984).

MINERALOGY

The mineralogy of quartz veins is fairly simple. Chalcopyrite occurs as the predominant sulfide mineral in all the veins of the area, associated with minor pyrite, galena, sphalerite, arsenopyrite and rare enargite, marcasite, digenite, bournonite, tetrahedrite, electrum, and supergene bornite and covellite. Detailed study of mineral relations in the field, in hand specimens, and microscopically reveals mineralization with a polyascendant character. Three stages of mineralization separated from another by tectonic breaks are recognized. Within an individual stage of mineralization, a definite sequence of mineralization of monoascendant character is observed (So and Chi, 1984).

Stage I is composed of quartz and minor amounts of chalcopyrite and pyrite, and rarely enargite, amethyst, and chlorite. Quartz is the most important gangue mineral and has a massive appearance. It is medium to coarse crystalline and fine-grained at the margins of the veins.

Pyrite occurs rarely in the form of fine to medium-grained disseminations throughout the veins, and frequently as aggregates of anhedral grains which are intimately intergrown with chalcopyrite at the edges of the veins. Pyrite commonly also occurs as fractured, granular aggregates filled by chalcopyrite.

Chalcopyrite is distributed irregularly throughout the vein as small anhedral masses with no regular outline. Often small (less than 5mm) subhedral to euhedral crystals of chalcopyrite occur in vugs.

Vein mineralization of stage I was followed by an episode of major gravity faulting along the vein strike. The faults may have contained open spaces prior to the introduction of the main orebearing quartz veins of stage II.

Stage II mineralization is economically the most significant and is divided into two separate cycles of mineralization. Stage IIa is characterized by an early, mostly transparent quartz associated with abundant sulfides, and stage IIb, by latter pale pinkish quartz associated with rare sulfides. Stage IIb, quartz is often observed overgrowing stage IIa quartz grains which protrude into open spaces. Infrequently veins of stage IIb quartz cut stage IIa quartz veins. These veins often contain stage IIa vuggy quartz (So and Chi, 1984).

Stage IIa is represented by mostly early quartz and chalcopyrite, and small amounts of pyrite, galena, sphalerite, arsenopyrite and fluorite, with rare enargite, marcasite, bournonite, terahedrite, electrum, and chlorite.

Transparent and occassionlly white stage IIa quartz is observed to cut stage I quartz and may enclose breccias of earlier vein materials. This suggests that reopening of fractures and some brecciation took place during stage IIa vein mineralization.

Pyrite forms subhedral to euhedral grains intergrown with chalcopyrite and galena. Fine euhedral grains are commonly disseminated in the host-rock welded tuff and clay minerals developed along faults. Irregular corroded margins are commonly observed on pyrite where chalcopyrite, galena, and sphalerite have replaced pyrite by advancing along irregular cracks. Some of the highly brecciated pyrite fragments are cemented by galena and chalcopyrite.

Chalcopyrite, the dominant copper mineral in the mines, is present as small anhedral disseminations and forms irregular veinlets. It is also found as anhedral grains intergrown with other sulfides. It is noteworthy to observe the zoning of chalcopyrite mineralization in veins. From the margins of veins to central vugs, chalcopyrite is associated with pyrite in the marginal zone, with pyrite-galena-sphalerite in the intermediate zone, and with galena in central vugs. This suggests that deposition of chalcopyrite took place over a long period. Rarely, galena, sphalerite and chalcopyrite crystal masses have grown out directly from the wall rocks of the vein. There are large residual fragments of hostrock welded tuff which have escaped replacement, and these are traversed irregularly by small stringer veins of quartz and chalcopyrite.

Galena is coarse-grained (greater than 5mm) and occurs as anhedral polycrystalline aggregates intergrown intimately with sphalerite and chalcopyrite. It is commonly interstitial to pyrite and sphalerite. Galena often occurs as cubeoctahedra associated with euhedral chalcopyrites in vugs. Sphalerite occurs as iron-poor and iron-rich varieties (to 9.5wt.% Fe) which range in color from dark brown to black (So and Chi, 1984).

Arsenopyrite is commonly observed as euhedral to subhedral crystals with characteristic rhombohedral shapes in pyrite grains and is replaced by galena. Enargite occurs as drop-like inclusions in pyrite. Marcasite occurs as lamellar intergrowths with pyrite. Bournonite occurs rarely near the margins of chalcopyrite. Electrum infrequently occurs in galena penetrating pyrites.

Calcite occurs rarely in small amounts rhythmically overgrowing quartz in vugs.

Stage IIb barren quartz veins are characterized by pale pinkish quartz and small amounts of amethyst, with minor or fine-grained disseminated chalcopyrite and pyrite.

The latest phase of tectonic activity occurred after mineralization of the stage Ⅱ veins. Post-ore

faults have been filled with calcite and minor amounts of fine-grained pyrite in vugs. These calcite veins develop within some of the pre-existing veins with variable attitudes.

REFLECTION CHARACTERISTICS OF THE ORE MINERALS

Instruments

MPV microscope photometer was used in conjunction with an Ortholux-Pol microscope, accurately adjusted to give normally incident plane polarized light. The MPV photometer has an EMI photomultiplier 6094A (Knott Dlektronik, Munich). The output from the responding photomultiplier was recorded on a moving spot galvanometer (NORMA) of 2K ohms internal resistance and full scale deflection of 0.018 A on its most sensitive scale. The light source for all observations was a 12 volt 100 watt halogen lamp, operating at a color temperature of about 3,400 K. For stabilization of the light source, a transistor stabilizer (Knott Elektronik) was connected in parallel with the lamp. The resulting light intensity and the sensitivity of the photomultiplier were sufficient to allow monochromatic determinations to be made by interposing a series of Leitz interference filters of a half-value width of about 200 and of a maximum transparency of about 60%, between the light source and vertical illuminator tube. All determinations were made under x 16, 0.40 N.A. in air and x 12.5, 0.25 N.A. in oil, strain-free objectives, carefully centered. Under these operating conditions. the photomultiplier output varied between 0.4–0.6 R% according to the surface measured and wavelength employed. Operation of the lamp iris controls the effective numerical aperture of the objective, so it was closed down to a constant small value to reduce the effects of obilque incidence. A neutral density filter was used for rough control of the light intensity. The final control was achieved by adjusting the photomultiplier gain.

Measurement Procedure

Sample preperation

One of the important error sources in reflectivity measurement is the polished surface condition of the specimen. Perfection of polish, cleanliness of the surface, and time since polishing are extremely important variables. Imperfections in polishing, and tarnish, limit the accuracy of the determinations to a greater extent than any other variable. If the surface is not perfectly normal to the incident beam, light can be lost with scattering from surface imperfections. Care was taken always to ensure that the surface over the area on which the beam falls is flat, and also that it is normal to the axis of the microscope.

Cut slices or separated grains were moulded in an epoxy resin. Grinding was then carried out in four different stages on a cast-iron lap in a slurry of SiC-powder and water; the grades of SiC-powder used were: SiC–280, SiC–400, SiC–600, SiC–1000.

The rough polishing stages were performed on a petrodisc, a cast aluminium disc coated with a partly self-lubricating hard plastic layer. This disc gives rise to practically no relief. Buehler polishing cloths (nylon, AB Texmet, and Texmet) were used with polishing abrasive Metadi 9μ, 6μ, 3μ, 1μ, $1/4\mu$ and 0.05μ on the Buehler polishing table. Hand polishing with soft tissue and no abrasive produced a rather better result on the polished surface.

Accuracy

Much care was always taken to avoid the slightest movement of the microscope when the filter slides or the polarizers or other devices are handled or the microscope stage is rotated. However, errors caused by lack of mechanical stablilty were present in all measurements in reflected light. Under standard conditions, replicate determinations of reflectivity of the studied sphalerites (16.4–21.3%) give precisions of $\pm 0.2\%$ at the 95% confidence level. The measuement in yellow wavelength with our standard is subject to the

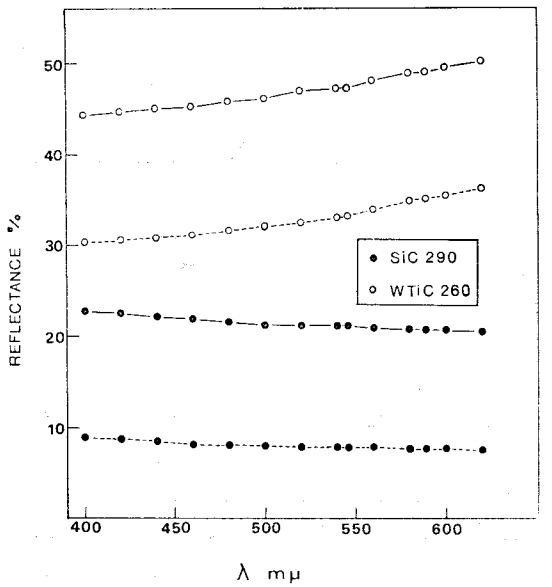

Fig. 1 Spectral reflectivity data of standard. solid line: measured in air, dashed line: measured in oil.

lower values of the range of errors, and the measurements in orange, green and blue wavelengths to the highest part of the range.

Standard

Regardless of the type of measuring system employed, one or more standard reference surfaces of known reflectivity are necessary. Number of the standards vary according to the characteristcs of the equipment, but at least two are required if a check is to be kept on the response linearity of the photomultiplier. Silicon Carbide (SiC 290) and Tungsten Titanium Carbide (WTiC 260) are used as the standards. For checking the linearity of the photomultiplier response, the reflectivities were measured against air and oil according to German standard DIN 58 884, and the results are shown in Fig. 1.

The relative standard deviation referred to the mean reflectance at a given wavelength is ±1.5%. The reflection of the standard seems to be stabilized to a constant value after about an hour (Fig. 2). However, after each measurement of the reflection of any specimen, the measured value had to be calibrated against the standard values in order

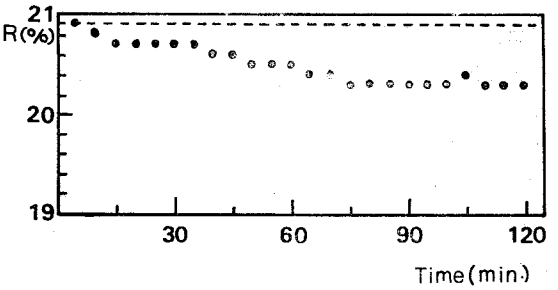

Fig. 2 Reflection of SiC 290 standard at 544mμ measured every 5 minutes on a specified position of the standard surface.

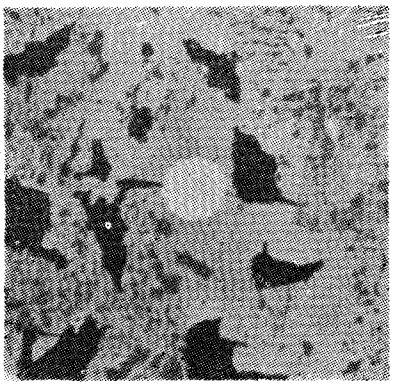

Fig. 3 Studied minerals with adjusted measuring iris diaphragm.

to reduce the error in measurements.

Reflectivity Measurement

The quantitative measurement of reflectivity under the microscope was made by comparing the intensity of light reflected by a specified mineral surface with that obtained from a standard surface of known reflectivity under the same conditions. The specimens are cleaned with zyrol, dried and placed on the plate and leveled with a hand-press. After allowing 45 minutes for the light source to reach steady intensity, a small, flawless area of the mineral was selected. The grain precisely focused with the aid of tiny pits or other minute imperfections of the surface outside the 40-micron circle.

The field-and tube-iris diaphragms were closed down to isolate a small area in the centre of the field. The whole optical system was left untouched until the set of measurements was completed. The section was then removed and replaced by the

standard, and the process repeated under identical conditions of illumination, with constant diameters of measuring and field irises (Fig. 3).

A neutral density filter was used for rough control of the light intensity, final control being obtained by adjustment of the photomultiplier gain. The actual reflectivity values were read off from the galvanometer reading for the appropriate wave -lengths with each of the filters in turn. For routine work, two or three measurements sufficed to obtain a useful value.

Since the ore minerals studied are anisotropic, as the stage is rotated a maximum reading for the grain (R_1) is obtained when one of its vibration directions is parallel to the polarizer vibration plane, and a minimum reading (R_2) when the other vibration direction is parallel to the polarizer vibration direction. At each position, the focus is carefully checked before the final reading is taken.

The optical symmetry of a given mineral can be partly determinod from its optical properties, chiefly reflectivity and anisotropism or isotropism (Cameron, 1966). For determination of optical symmetry, a polished section containing numerous randomly oriented grains of the mineral was used, and uniradial reflectivity was measured at $\lambda=$ 544mμ directly by rotating the mineral on the stage until readings for minimum (R_1) and maximum (R_2) values were obtained.

Electron Probe Microanalysis

Fe content (wt. %) of the studied sphalerite specimens was analysed by a JEOL JXA-50A electron probe microanalyser.

Sepectral profiles and Its Relationship to White Light Color and Mineralization Sequence

For vertical incident light the reflecting power of a transparent isotropic substance may be expressed by the Fresnel equation:

$$R=\left(\frac{n-1}{n+1}\right)^2,$$

where R is the reflection percentage, n is the index of refraction of the mineral, and the absorption is assumed to be zero. Ore minerals absorb a considerable amount of the incident light. The value of R depends on the absorption, as well as on the value of n. It is convenient to use the absorption coefficient k to express the absorption. The equation of reflection in air now:

$$R=\frac{(n-1)^2+k^2}{(n+1)^2+k^2}$$

Isotropic minerals show a single spectral reflectivity profile that is constant in shape. But, since anisotropic species are bireflecting except for sections at 90° to the optic axis (uniaxial minerals) or rotation axes (orthorhombic, monoclinic and triclinic minerals), sections of these minerals show a range of reflectivity defined by two spectral reflectivity profiles.

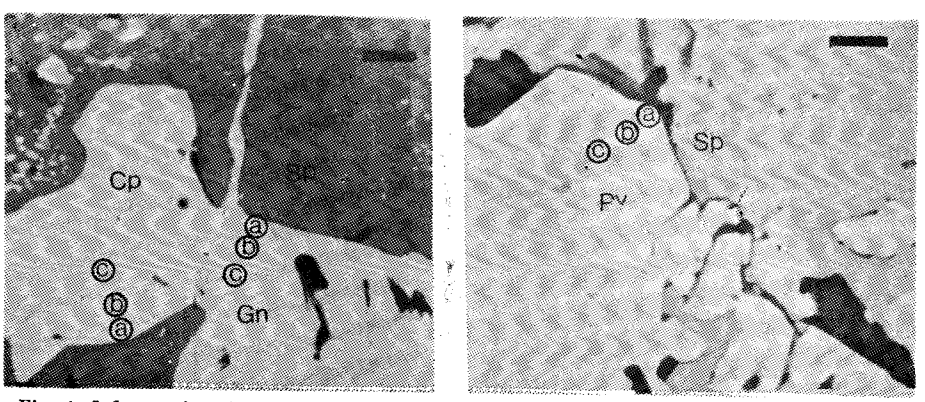

Fig. 4 Influence of neighboring sphalerite on the reflectivity measurement (at λ=544mμ) of (A) galena, chalcopyrite and (B) pyrite grains. Scale bar is 0.1mm. Abbreviation: SP=sphalerite, GN=galena, PY=pyrite, CP=chalcopyrite.

Table 1 Influence of neighboring sphalerite on the reflectivity measurement (at λ=544mμ) of galena, chalcopyrite and pyrite.

in air

Measured mineral	Distance from neighboring mineral	438 (Indigo)	504 (Blue)	544 (Green)	593 (Yellow)	615 (Red)
Chalcopyrite	a	22.6	40.0	44.8	47.5	48.2
Neighboring	b	23.2	40.1	45.5	47.9	49.6
mineral=Sphalerite	c	23.5	40.8	46.0	48.5	48.9
Galena	a	45.6	42.8	41.7	40.5	40.2
Neighboring	b	46.0	43.0	42.8	42.0	41.2
Mineral=Sphalerite	c	47.2	43.4	43.0	42.3	42.3
Pyrite	a	43.0	51.2	50.8	53.1	55.8
Neighboring	b	43.2	51.2	50.8	53.2	55.9
Mineral=Sphalerite	c	43.4	51.5	51.0	52.3	56.0

Assuming uniformity in the quality of the polished surfaces, variations in reflectivity within and between different specimens of a mineral species, in a given spectral region, are due to variations in orientation and/or composition (Gray and Millman, 1962).

The reflectivity of oriented and unoriented section of mineral species studied for paragenetic sequence, chemical composition and mineral orientation were measured at six regions in the visible spectrum (403mμ, 438mμ, 504mμ, 544mμ, 593mμ and 615mμ wavelength).

Optical dispersion effect caused by a neighboring mineral

The optical dispersion effect on the reflectance of a specimen surface caused by the presence of a neighboring mineral grain having a different reflectance was studied. In order to study the phenomenon, galena, pyrite and chalcopyrite grain in contact with a sphalerite was taken and measured (Table 1)-the latter has much different reflection from the former.

Fig. 4 presents that the measuring diaphragm on the measured minerals was penetrated step by step the sphalerite from c to a. Fig. 4 and 5 show influence of neighboring sphalerite on the reflectance measurement of galena, pyrite and chalcopyrite. The more penetrated the measuring diaphragm on the measured surface of the studied minerals into sphalerite, the more decreased reflectance value of the measured minerals. Galena has the most optical dispersion than other minerals, depending on neighboring sphalerite with lower reflection power.

Dependence of reflection power on Mineralization sequence

Reflectivity measurements in air and in oil were made on chalcopyrite, pyrite, galena, sphalerite, marcasite, arsenopyrite, enagite for mineralization stage I and II. All reflectance values of the studied mineral species are summarized in Table 2 and are shown graphically in Fig. 6–8.

In Fig. 6, stage I and II chalcopyrite in air, deep yellow in white light, represents steeply progressive increase in reflectivity until yellow wavelengths, showing a slight depression around 438mμ in the profiles. These have a similar profiles in shape. In air, stage II chalcopyrite has slightly higher reflectance value than stage I chalcopyrite. Stage II chalcopyrite indicate more strong bireflectance at each wavelength than stage I chalcopyrite and does not show absorption band at 438mμ wavelength in oil.

In air, pyrites, pale yellow in white light, show in general a steeply progressive increase in profiles towards orange wavelengths. Pyrites studied indicate also clearly a weak bireflection. Stage I pyrite has slightiy higher reflectance value than stage II pyrite. (Fig. 7).

All reflectance value of other minerals measured in air and oil for the studied mineral species in

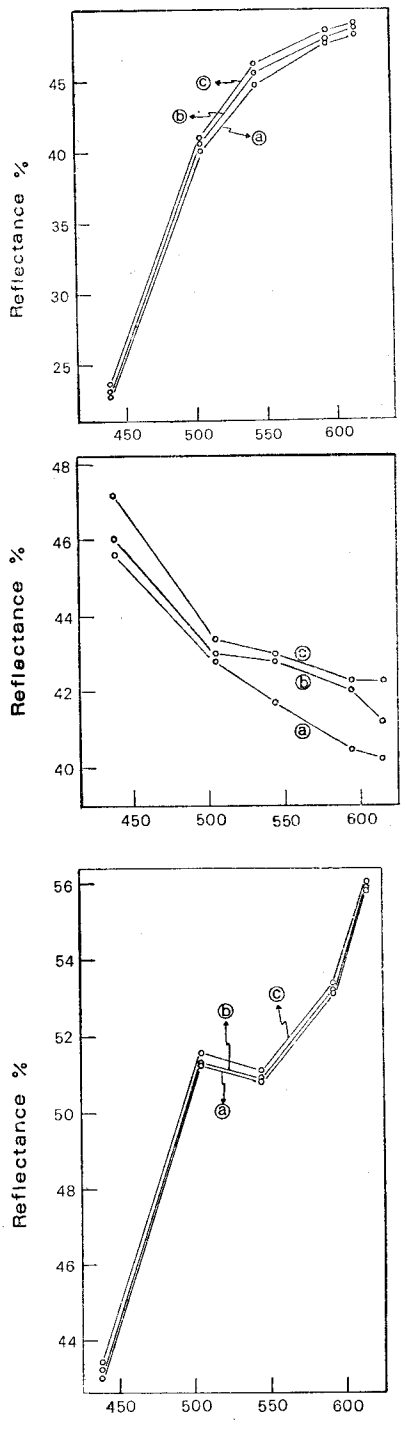

Fig. 5 Influence of neighboring sphalerite on the reflectance measurement of chalcopyrite, pyrite and galena.

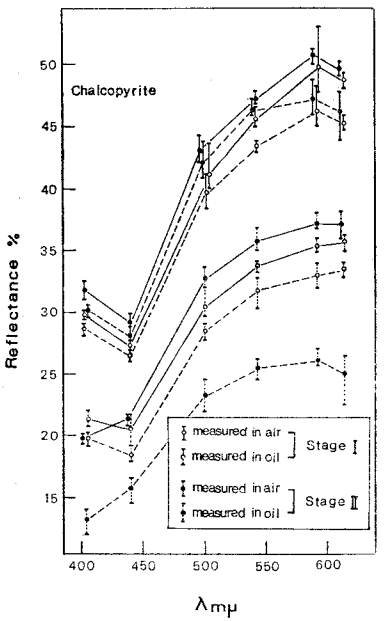

Fig. 6 Spectral profiles of unoriented sections of different stage chalcopyrite measured in air and oil. (solid line: maximum spectral dispersion, dashed line: minimum spectral dispersion)

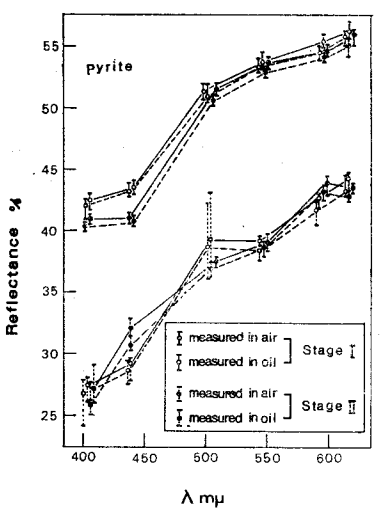

Fig. 7 Spectral profiles of unoriented sections of different stage pyrite measured in air and oil. (solid line: maximum spectral dispersion, dashed line: minimum spectral dispersion)

Table 2 Spectral reflectances (R_2/R_1) of the studied minerals for mineralization stages in air and oil.

Mineral	Mineralization stage	403 (violet) mμ		438 (indigo) mμ		504 (blue) mμ	
		air	oil	air	oil	air	oil
Pyrite	stage Ⅰ	41.1～42.5/41.7～43.0	24.2～28.0/25.6～28.3	42.9～43.8/43.1～44.0	27.2～29.4/27.8～30.2	50.5～51.8/51.0～52.0	36.8～42.4/37.1～43.3
	mean	42.0/42.5	26.7/27.3	43.2/43.5	28.6/29.2	50.9/51.3	38.7/39.4
Chalcopyrite	stage Ⅰ	28.3～28.9/29.8～30.0	19.4～20.1/20.8～22.0	26.2～26.8/27.0～27.5	18.1～19.2/19.8～21.2	38.5～41.3/40.0～43.2	27.7～29.1/29.8～32.0
	mean	28.6/29.9	19.8/21.3	26.5/27.2	18.8/20.5	39.7/41.2	28.6/30.6
Pyrite	stage Ⅱ	40.2～40.4/40.8～41.4	24.2～27.9/25.8～29.0	40.2～41.0/40.8～41.2	31.0～31.3/32.1～33.0	50.4～51.0/51.2～51.3	36.7～37.2/37.2～37.6
	mean	40.3/41.1	25.9/27.1	40.4/41.1	31.0/32.2	50.8/51.8	37.1/37.4
Chalcopyrite	stage Ⅱ	29.6～30.4/31.0～31.7	12.0～14.0/19.5～19.8	27.7～28.0/28.8～28.9	14.5～16.5/20.9～21.5	40.8～42.1/42.2～43.0	22.0～24.5/31.6～33.6
	mean	30.1/31.7	13.3/19.7	27.9/28.9	15.6/21.3	41.2/43.0	23.3/32.6
Marcasite	stage Ⅱ	36.0～40.4/38.5～41.1	25.8～27.0/27.2～30.1	40.6～42.5/40.9～45.5	30.0～32.2/32.3～36.0	48.2～50.6/51.4～54.1	35.0～37.0/37.5～39.0
	mean	36.1/38.6	26.0/29.8	42.3/45.4	31.1/35.5	48.7/54.0	35.5/38.0
Enargite	stage Ⅱ	30.1/32.4	13.5/20.0	28.8/29.6	16.0/21.5	43.8/44.2	24.0/33.0
Arsenopyrite	stage Ⅱ		19.7～20.0/22.1～25.0		27.6～28.1/32.4～34.5		27.1～30.0/34.8～35.5
	mean		19.8/23.8		27.9/33.4		28.6/35.2
Galena	stage Ⅱ	46.8～47.0	28.0	45.2～47.0	29.8～31.8	42.2～44.0	27.1～28.6
	mean	46.9	28.0	45.2	30.8	43.2	28.1
Sphalerite	stage Ⅱ	18.0～18.2	4.3～5.1	17.1～17.3	5.1～5.2	16.3～16.5	4.6～4.8
	mean	18.1	4.7	17.2	5.2	16.4	4.7

Table 2 Spectral reflectances (R_1/R_2) of the studied minerals for mineralization stages in air and oil.

Mineral	Mineralization stage	544 (green) mμ		593 (yellow) mμ		615 (red) mμ	
		air	oil	air	oil	air	oil
Pyrite	stage Ⅰ	53.0~54.0/53.2~54.5	38.0~38.8/39.0~39.3	54.1~54.9/55.2~55.8	38.2~39.9/39.1~40.9	55.0~56.1/55.6~56.0	39.8~41.8/40.8~42.2
	mean	53.3/53.7	38.4/39.1	54.6/55.4	39.2/40.1	55.7/55.8	40.9/41.7
Chalcopyrite	stage Ⅰ	43.0~43.5/45.0~46.5	30.3~32.8/33.4~34.0	44.9~48.2/47.8~53.0	32.0~33.9/34.9~35.9	44.8~45.8/48.1~49.3	33.0~33.9/35.0~36.2
	mean	43.3/45.5	31.7/33.8	46.3/49.6	33.0/35.3	45.3/48.6	33.5/35.7
Pyrite	stage Ⅱ	52.5~53.0/53.2~53.8	37.9~39.0/38.2~39.6	53.8~54.5/54.2~55.1	39.8~41.1/40.4~41.9	54.2~54.8/55.0~56.2	40.0~40.8/40.8~41.2
	mean	53.0/53.6	38.8/39.2	54.2/54.7	41.0/41.8	54.6/56.0	40.3/41.2
Chalcopyrite	stage Ⅱ	46.1~46.2/46.9~47.2	24.5~26.1/35.1~36.9	46.0~48.7/50.0~51.2	25.1~27.0/36.8~37.9	43.8~46.0/49.2~50.2	22.5~26.5/36.0~37.5
	mean	46.1/47.2	25.4/35.9	47.2/50.7	26.1/37.2	45.1/49.6	25.0/37.2
Marcasite	stage Ⅱ	47.0~52.8/50.5~53.6	35.5~38.6/39.0~40.0	51.5~54.1/54.8~56.5	35.5~40.7/41.0~41.5	53.0~55.1/55.8~55.9	39.0~41.2/41.1~45.1
	mean	47.5/51.3	35.7/39.8	52.3/56.5	36.8/41.1	53.5/55.9	40.1/43.2
Enargite	stage Ⅱ	47.1/47.8	26.0/36.1	47.0/50.9	26.0/37.1	46.8/50.2	25.0/38.2
Arsenopyrite	stage Ⅱ		24.9~30.3/35.8~36.8		22.0~29.0/30.1~35.8		20.0~23.0/30.9~32.3
	mean		28.1/36.2		25.3/33.3		21.9/31.4
Galena	stage Ⅱ	41.0~42.8	27.2~28.2	41.0~42.5	27.4~28.9	41.8~42.8	26.1~27.1
	mean	42.2	27.8	41.8	28.4	42.3	26.7
Sphalerite	stage Ⅱ	16.0~16.1	4.7~4.8	16.2	4.5~4.6	16.0~16.1	5.2~5.3
	mean	16.1	4.8	16.2	4.6	16.0	5.2

stage II are shown graphically in Fig. 8.

Marcasite, pale yellow under the microscope, shows a steeply progressive increase toward orange wavelengths, showing absorption band at 544 (green) mμ in air, and indicates the strongest bireflectance at each wavelength among the mineral species studied. Arsenopyrite, white with pale-creamy in white light, presents progressive increase in reflectivity until green wavelengths and decrease steeply towards orange wavelengths, and shows more strong bireflectance value towards orange wavelength in oil

Galena studied, grayish white in white light, shows decrease in reflectivity towards orange wavelengths, but, represents broad depression in oil. Enargite, pale brown in white light, shows generally a progressive increase in profile towards orange wavelengths and indicates very strong bireflectance. Sphalerite, bluish gray in white light, shows relatively flat profiles and slightly decrease in reflectivity towards orange wavelength. Reflection power of sphalerite is the lowest in air and oil, than any other stage II mineral species at different waveleng ths.

The reflectance variation depending on mineralization sequence are resulted from variation of structure and composition due to different physico-chemical conditions in time during the complex cooling history of the entire hydrothermal system.

Dependence of Reflection Power on Chemical Compositions

Reflectivity variation on chemical compositions was performed by Squair (1965) and by Eales (1967) for determining the silver content of natural gold-silver alloys. Cervelle, Levy, and

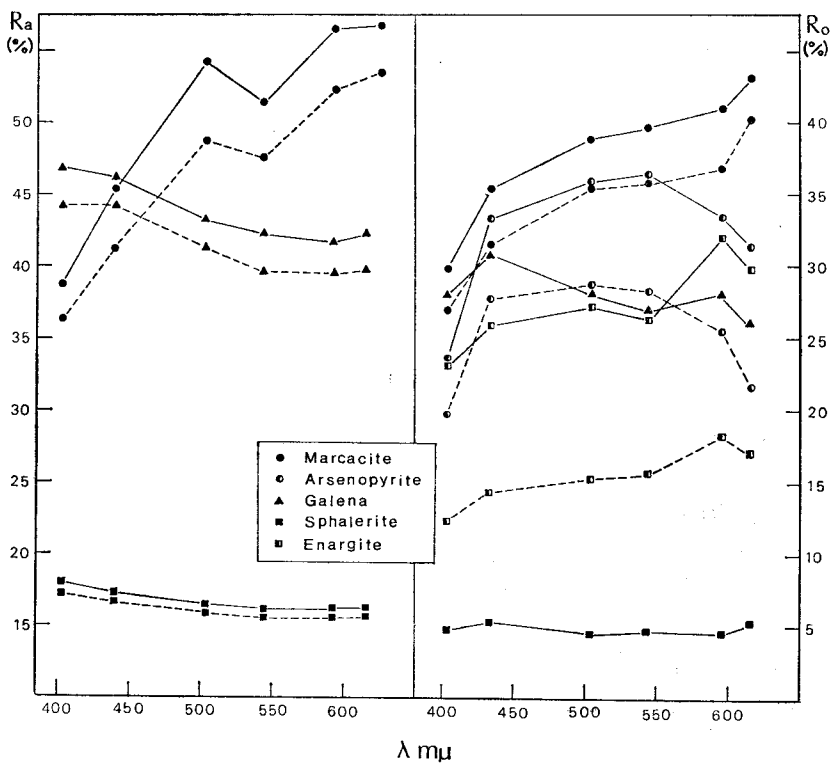

Fig. 8 Spectral profiles of unoriented sections of stage II minerals (marcasite, galena, sphalerite, arsenopyrite, enargite). Solid line: maximum spectral dispersion, dashed line: minimum spectral dispersion.

Table 3 Spectral reflectance against the Fe content (wt. %) for the studied sphalerite in air and oil.

Fe content (wt. %)	403(violet)			438 (indigo)			504 (blue)			544 (green)			593 (yellow)			615 (red)		
	air	oil	n	air	oil	n	air	oil	n	air	oil	n	air	oil	n	air	oil	n
8.87	17.3	7.0	1.99	17.0	5.8	2.22	16.8	5.2	2.33	16.8	4.0	2.73	16.6	5.8	2.13	17.0	5.0	2.45
8.05	17.2	6.5	2.09	17.1	6.1	2.16	16.1	5.0	2.23	16.0	3.8	2.55	16.4	5.2	2.24	16.9	4.5	2.58
9.5	17.8	6.9	2.11	17.7	6.0	2.33	16.9	5.7	2.22	16.8	4.0	2.73	17.0	6.0	2.17	17.1	5.0	2.19
1.48	18.7	7.0	2.29	17.4	5.7	2.34	16.3	4.8	2.33	15.0	4.0	2.49	15.9	4.3	2.37	16.0	4.4	2.37
1.46	18.0	8.0	1.91	17.3	5.6	2.34	16.4	4.7	2.38	15.9	4.0	2.46	15.9	4.3	2.40	16.0	4.4	2.37

Caye (1971) have studied the effect of magnesium subsititution on the reflectance.

Vaughan (1973) observed a general increase in average reflectance with increasing metal defici-

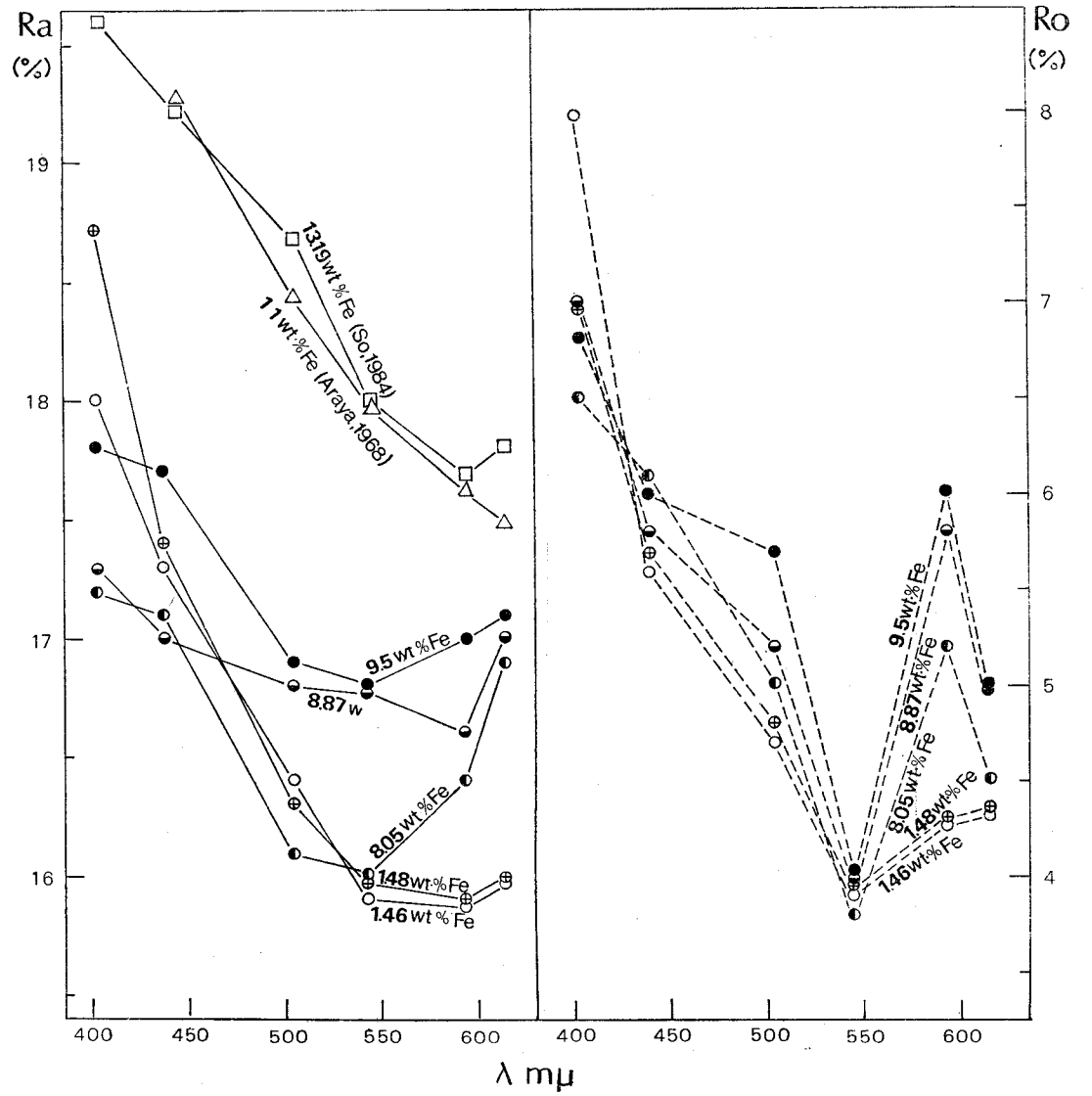

Fig. 9 Spectral reflectance, in air and oil, plotted against the Fe content (wt. %) for the studied sphalerite (solid line: measured in air, dashed line: measured in oil) and compared to the data after So (1984) and Araya (1968)

ency in a series of synthetic samples, and Carpent and Bailey (1973) demonstrated that measurement of Ro (at 546 nm) could be used to distinguish troillte from "hexagonal" or intermediate pyrrhotite and either of these from monoclinic pyrrhotite. In the mineralogically very complex series of compositions related to the tenantite-tetrahedrite group, Charlet and Levy (1976) have examined the reflectivities as a function of complex chemical substitutions in compositions of the type (Cu, $Ag)_{10}$ (Cu, Fe, Zn, $Hg)_2$ (As, $Sb)_4$ S_{13}, other examples of this systematic approach to the relationship between reflectance and chemical composition include studies of the sulfosalt of Copper(Levy, 1967), of platinum minerals (Stumptl and Tarkian, 1973), of the homogeneous and exsolved titanomagnetite (Halfem, 1976) and of the silver sulfosalt (Pinet et al. 1978).

So (1977, 1984, a and b) has studied the dependence of Korean sulfides-oxides reflectances on their major and minor compositions. In this study reflectivity dependence of the studied sphalerite and their iron content was investigated in detail. Five sphalerite grains were quantitatively analysed for Fe content (wt, %) by a JEOL JAX-50A electron probe microanalyser.

Table 3 gives the obtained reflectivity values, refractive indes, and Fe contents in sphalerite. Fig. 9 shows spectral reflectance, in air and oil, plotted against the Fe contents for the sphalerites.

Close relationship between the reflectance and compositions was found. The reflection power of the studied sphalerite increase proportionally with the substituting Fe content (wt. %) for Zn at

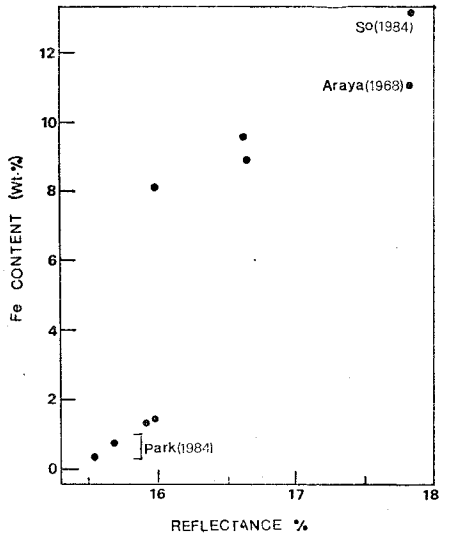

Fig. 10 Plot of reflectance (at λ=544mμ) against Fe content for sphalerite.

different wavelength (>504mμ) in air and oil (Fig. 9).

In Fig. 10 the R_{504} values are plotted against Fe content, since the photomultiplier used was most sensitive at 504 mμ, this wavelength was chosen to illustrate variation in reflectivity. Although the amounts of Fe content in the sphalerites studied are small, and the variation is restricted, the results show a good correlation.

Dependence of reflection power on Mineral Orientation

Reflectance will commonly vary as a function of crystallographic orientation at the polished surface relative to the vibration direction of the linearly polarized incident light. Table 4 presents the spectral reflectance (%) of the oriented sections

Table 4 Spectral reflectance(%) of the oriented sections //(111) and //(100) of the sphalerite.

Wavelength(mμ) / Mineral orientation	403 (violet)		438 (indigo)		504 (blue)		544 (green)		593 (yellow)		615 (orange)	
	in air	in oil	in air	in oil	in air	in oil	in air	in oil	in air	in oil	in air	in oil
//(111)	18.1	5.8	17.0	5.2	16.2	4.9	15.6	5.0	15.9	4.2	15.6	4.2
//(100)	18.0	5.9	17.2	5.4	16 5	4.9	15.8	5.2	15.9	4.3	16.0	4.6

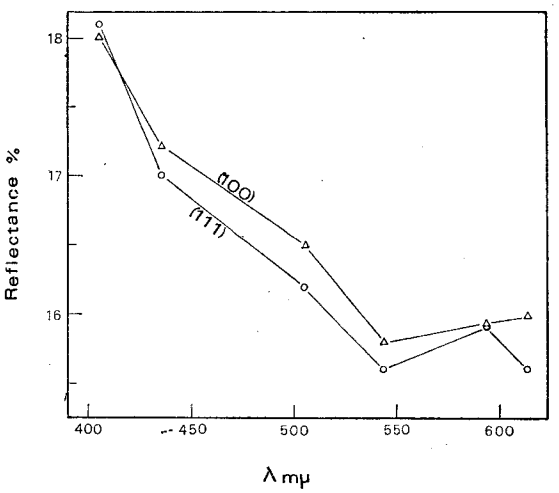

Fig. 11 Spectral reflectance(%) on (111) and (100) of the sphalerite measured in air.

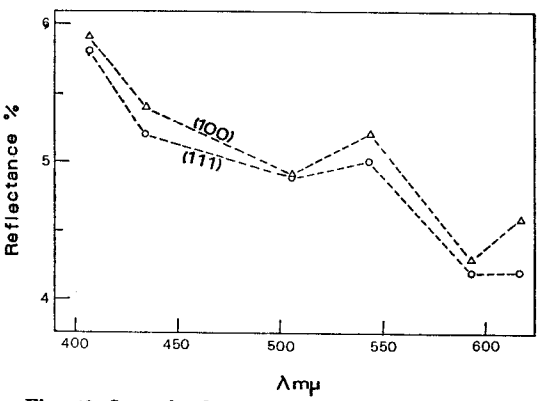

Fig. 12 Spectral reflectance (%) on (111) and (100) of the sphalerite measured in oil.

//(111) and //(100) of the studied sphalerite.

In Fig. 11 and 12, the spectral reflectances on the surface of //(111) polished crystal faces are clearly higher 0.4% in air 504 mμ than those on the surface of //(100) crystal surface of sphalerite.

Effect of Internal Reflection on Reflection Power

Sphalerite commonly shows apparent bireflection and exhibits under open Nicols different internal reflection colors with variation of chemical impurities. At about 10 per cent Fe the mineral becomes opaque, and internal reflections can no longer be observed (Stanton, 1972). The intensity and nature of the colors vary from white to pale amber in low iron-manganese varieties through various shades of red to deep ruby as iron and/or manganese increase. Consequently sections of the sphalerites with internal reflection show a range of reflectivity, resulting in sympathetic variation in the shape of profiles. (So, 1984a)

In order to study the effect of internal reflection on the reflection power of the sphalerite, six specimens which clearly showed internal reflection were examined.

Reflectivity of portion on the sphalerite specimens where internal reflection could be observed and on the same grain, not showing internal reflection, were measured at λ=403, 438, 504, 544, 593 and 615 mμ under parallel nicols in oil (Table. 5).

In Fig. 13 the spectral profiles of the sphalerite which have various internal reflection colors show more variation than the specimens, not showing internal reflection. The reflectivity value of the mineral at which the internal reflection was observed, were different from the normal value.

Sphalerite, showing green, yellow and reddish brown internal reflection have the highest reflection power at 544mμ (green), 593mμ (yellow), 615mμ (red), respectively.

Table 5 Reflectivities of sphalerites (in oil) with different internal reflection colors.

Wavelength (mμ) / Color	403 (violet)	438 (indigo)	504 (blue)	544 (green)	593 (yellow)	615 (red)
Yellow	5.5	6.0	4.9	4.0	5.4	5.0
Greenish-yellow	6.8	6.0	5.0	4.5	4.7	4.3
Orange	6.9	6.1	4.1	4.3	4.5	4.7
Green	4.8	5.5	4.2	5.2	4.4	4.2
Reddish brown	6.9	5.9	4.9	5.0	5.2	5.3
Rainbow	6.1	5.3	5.1	5.0	5.0	4.8

Optical Symmetry

Apparent uniradial reflectance of randomly oriented grains of bireflecting ore mineral is measured at 544 mμ (Table 6). Reflectivity data for the studied tetragonal mineral (chalcopyrite) is given

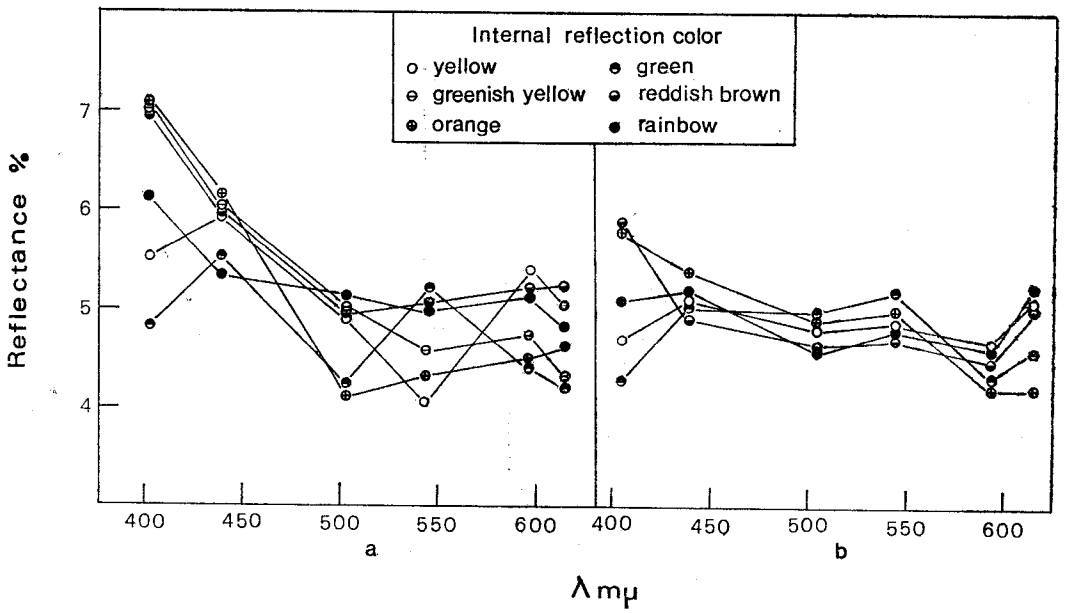

Fig. 13 Spectral dispersion of sphalerite with various internal reflection color under //nicols(a) measured in air, compared to reflectances on the same grain, not showing internal reflection(b).

in Fig. 14.

Each line of a figure represents, to scale, the bireflectance of a single grain. The end points of the line give the values of R_1 and R_2 for the grain. Even assuming an error of measurement of as much as 0.8 percent, the measurements indicate that none of the minerals is R_1 or R_2 constant, and that the minerals cannot be uniaxial. For any grain, R_1 may have any value between R_α and R and R_2 may have any value between R_β and R_γ. Provided the values of R_β–R_α and R_γ–R_β are large relative to the error of measurement, the biaxial character of the mineral should be evident from reflectivity measurements.

If the mineral is sensibly of lower symmetry there should be minimum, intermediate, and maximum values of R corresponding to the three coordinate either axis directions (paralled to a, b and c). If we designate these values of R as respectively R_1, R_m and R_g then R_m corresponds to R_β in transparent minerals. Then a diagnostic value of R can be determined.

For chalcopyrite, R_1 and R_2 were determined for 15 grains; The data plotted are for the grains selected as illustrating the range of values. Apart

Table 6 Reflectivity measurements of the studied chalcopyrite and arsenopyrite at 544nm.

Grain No.	Chalcopyrite	
	Re′	Rw
1	43.1	45.9
2	43.0	44.0
3	46.0	47.5
4	45.5	46.8
5	44.2	45.8
6	45.8	47.8
7	43.3	46.0
8	42.2	45.9
9	42.8	45.8
10	43.2	46.5
11	47.1	47.8
12	46.1	47.0
13	45.6	46.9
14	46.1	47.2
15	43.4	46.5
Mean Rw	46.50	
Mean deviation	0.75	
Range Re	42.2—47.1	
optic sign	—	

from the indication that they give of non-uniaxial character, we can see, in Fig 15, that for every mineral the pattern of variation of R_1 and R_2 from grain to grain is the same as would be expected if the minerals were transparent. Each grain of chalcopyrite shows a value of R_1 that is equal to or less than 45.9 ± 0.1 and a value of R_2 that is either equal to or greater than 45.9 ± 0.1. This value was taken as the R_β value as suggested by Cameron (1963). Since this value is evidently closer to the maximum value for the mineral (R_α) than to the minimum value (R_β), chalcopyrite would be indicated as optically negative (Fig. 17).

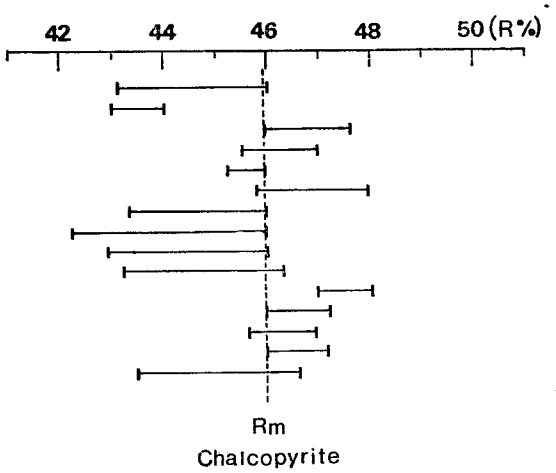

Fig. 14 Reflectance of diversely oriented grains of chalcopyrite.

Refractive Index and Its Dependence on Composition

From Fresnel's formula for reflectivity the following formulae for n can be derived: $n=0.5\ (n_0^2-1)\ (1-R_a)\ (1-R_0)/N\ (1-R_a)\ (1+R_0)-(1+R_a)\ (1-R_0)$ where R_a is the reflectivity in air, R_0 the reflectivity in oil, and n the refractive index of the immersion oil ($n=1.515$ for the present study). The calculated values of n for the minerals studied are shown in Table 2 and 3.

Fig. 15 shows the relation between the calculated values of n and composition of the sphalerite studied at 544 mμ. The n-values of sphalerite tend

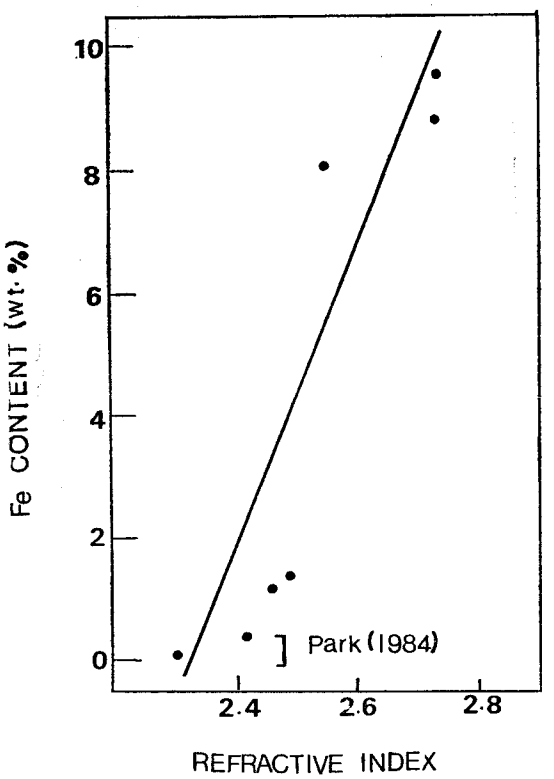

Fg. 15 Refractive index (n) plotted as a function of the Fe content (wt. %) of sphalerite.

to progressively increase with Fe content (wt. %)

MICROHARDNESS CHARACTERISTICS OF THE ORE MINERALS

The measurement of Vickers hardness provides an established and tested method for quantitative determination of the mineral hardness in polished section. The chief factors governing microhardness are the inter space-lattice structure of the minerals, the nature of the chemical bonds operating between the various atoms or ions, relative solubility, and stability (Nakhlar, 1956). The Vickers hardness values were made by applying various testing loads ranging from 25 to 300 grams (So, 1977, 1984, a and b).

Instruments

All measurements of microhardness impresent study (HV) were conducted with the Miniloadh-

Table 7 Vickers microindentation hardness measured for the unoriented sections of the different mineralization sequence

Minerals	Mineralization stage		25gr	50gr	100gr	200gr	300gr	Mean Value
Pyrite	stage Ⅰ	m HV	5.6～5.9/6.3～6.9 1168.1～1245.7	8.4～9.1/7.8～8.6 1170.6～1413.2	10.4～12.6/11.4～12.5 1168～1560.8	17.8～18.4/17.1～18.0 1182～1182.5	21.5～22.6/21.7～22.4 1139.0～1147.4	
	mean	m HV	5.8/6.6 1206.9	8.8/8.2 1291.9	11.5/12.0 1364.4	18.1/17.6 1182.3	22.1/22.1 1143.2	1237.7
Chalcopyrite	stage Ⅰ	m HV	14 9～15.2/15.0～15.5 195.5～206.0	21.5～22.0/21.6～23.5 173.8～198.7	30.4～32.3/30.6～32.8 176.6～199.3	45.3～47.7/45.5～49.5 158.3～179.0	49.8～55.5/50.7～57.5 174.8～219.9	
	mean	m HV	15.1/15.3 199.8	21.8/22.5 186.9	31.6/31.7 184.2	46.2/47.0 171.4	53.6/54.5 191.8	186.8
Pyrite	stage Ⅱ	m HV	5.5～6.3/5.9～6.5 1245.9～1331.8	7.1～9.9/8.1～9.2 1072.0～1378.9	12.0～13.3/11.8～13.2 1097.3～1287.8	17.0～18.6/14.8～18.4 1170.6～1329.8	23.9～25.1/22.3～26.6 829.3～1042.6	
	mean	m HV	5.8/6.1 1288.5	8.8/8.8 1198.5	12.5/12.5 1184.4	17.6/16.7 1261.2	24.6/24.7 923.1	1189.6
Chalcopyrite	stage Ⅱ	m HV	14.9～15.1/15.1～15.8 195.5～206.0	21.0～25.0/21.3～25.9 142.6～206.3	31.1～31.9/31.1～32.2 181.1～191.7	43.9～45.7/44.9～46.1 178.4～188.1	51.4～56.9/53.1～58.4 167.1～203.4	
	mean	m HV	15.0/15.4 201.6	23.3/23.7 172.7	31.4/31.7 185.8	44.9～45.7 180.8	54.6～55.9 182.8	185.0
Sphalerite	stage Ⅱ	m HV	15.4～15.7/15.7～15.8 185.7～190.5	21.9～22.3/22.3～22.9 181.5～189.8	31.9～34.2/32.3～34.4 157.6～180.0	44.8～45.7/45.2～46.1 176.8～183.2	54.4～59.9/57.3～61.9 150.0～173.7	
	mean	m HV	15.6/15.7 188.1	22.0/22.5 185.4	32.7/33.4 169.6	45.2/45.7 179.5	57.0/59.3 164.9	177.5
Galena	stage Ⅱ	m HV	25.0～26.3/25.0～26.2 67.0～74.2	35.4～38.5/35.5～39.1 61.6～73.6	50.9～53.5/50.5～54.3 63.8～72.1	72.2～75.9/72.6～76.3 64.0～70.8	90.6～100.0/94.2～98.4 56.2～64.3	
	mean	m HV	25.5/25.7 70.6	36.7/36.9 68.8	51.9/51.9 69.1	73.6/74.0 68.2	94.7/96.0 61.3	67.6

m: length of Vickers diagonal in micron
HV: Vickers-hardness in kg/mm^2

ardness tester, manufactured by E. Leitz. Ltd., Wetzlar. The design of the MINILOAD provides for a controlled rate of load application so that the indenter may be impressed into the test specimen without detectable impact effect and with a minimum possibility of fracturing brittle materials, an especially significant feature in mineral determinations. The rate of loading is controlled by means of a small hydraulic damper. The four-sided diamond shaped pyramidal indenter can be applied to grains as small as 2~3 micron in diameter and the apex angle between the opposed surfaces is 136°, while the depth of penetration equals one seventh (1/7) of the indentation diagonal.

Measurement Procedure

The microhardness test was conducted at the identical area on which the reflectivity measurement was undertaken by applying various test loads ranging from 25 to 300 grams. The rate of descent of the diamond has to be readjusted each 15–20sec., since temperature fluctuations affect the viscosity of the oil. Then indentation was done by bringing the diamond in contact with the studied mineral grain and applying a known load. After the indentation had been made, the stage was returned to the viewing position. The length of the two diagonals of the indentation was then read by means of a precision micrometer ocular (X40).

By knowing the test load applied in grams and the mean value of the indentation diagonal in 0.001mm., Vickers hardness is determined from the following equation:

$$HV\,(kg/mm^2)=\frac{1854\times t}{d^2}$$

t=test load in grams

d=length of the diagonal in microns

$2=\sin\frac{\alpha}{2}10^3=1854.4$ vickers constant(136°)

All measurements for reflectivity and microhardness were conducted under the following conditions: (1) A vibrationless working room.

(2) A room temperature of about 25°C.

(3) Clean working room, free from dust, vapor, and acids.

(4) Slightly darkened room.

The relative error of Miniload against the mean microhardness value of a hardness test plate and a test certificate by MPA Dortmund is ±1.1% at 100g and ±1.5% at 15g.

Dependence of Microhardness on Mineral Sequence

The Vickers micro-indentation hardness values for the studied pyrites and chalcopyrites are presented in Table 7. Fig. 16 shows the variation of vickers microhardness of pyrite and chalcopyrite for stage I and II with the various testing loads. The pyrite specimens examined have hardness ranging from 1182.1 to 1182.5 for stage I and for stage II from 1170.6 to 1329.8 under 200gr. load. Microhardness values of stage I and II chalcopyrite range from 158.3 to 179.9 and from 176.0 to 188.1 under 200gr. load respectively.

Fig. 17 illustrates the relation between the Vickers hardness (kg/mm²) of the other studied minerals (stage II) and test load.

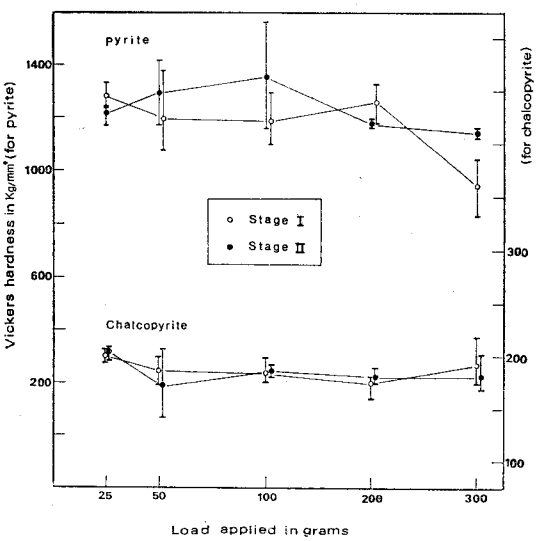

Fig. 16 Variation Vickers microhardness for Stage I and II pyrite and chalcopyrite with the various test loads.

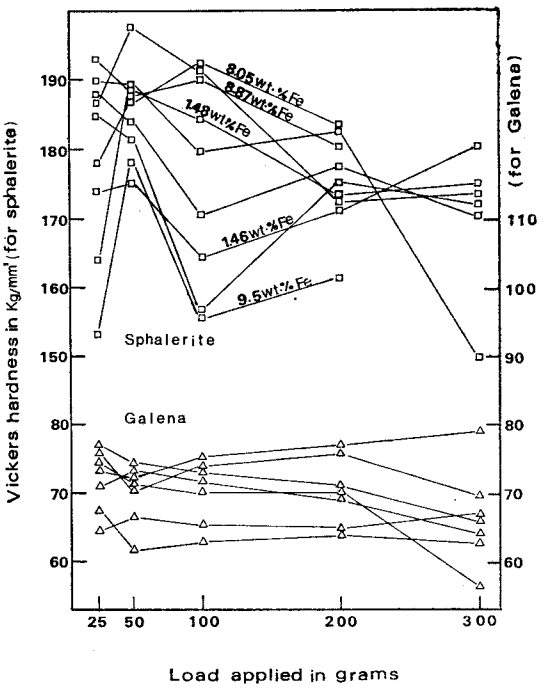

Fig. 17 Various Vickers hardness value for the studied sphalerite and galena with the various test loads.

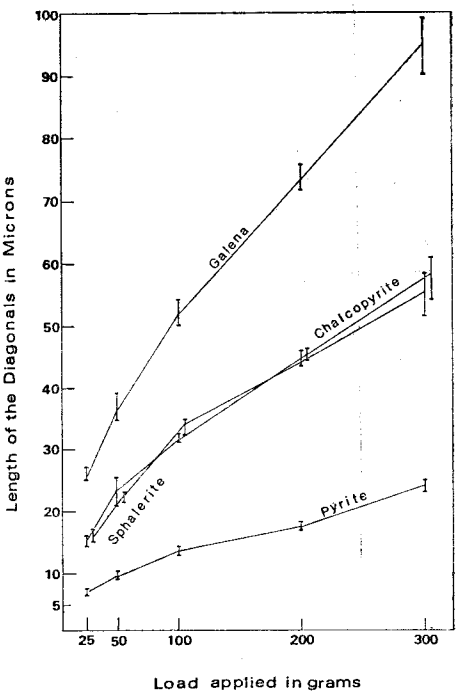

Fig. 18 The length variation of the indentation on the studied minerals with various test loads.

Sphalerite specimens studied have hardness ranging from 16.2 to 183.2 under 200gr. load. Galena, with relatively flat profiles, have hardness ranging from 63.2 to 77.9 under 200gr. load.

Length Variation of The Diagonal

The softer sulfides have the wider variation of the diagonal length at each test load. The variation increases with the test load for a mineral species. Fig. 18 shows the relation between diagonal length of the studied minerals and test load. Meter (1951) suggested that the higher the iron content the harder the mineral .They pointed out that more than 70 percent of the opaque minerals of Bi and Pb are soft minerals, and more than 75 percent of the opaque minerals of Fe are hard.

For some sulfide and oxide species variation of the diagonal length increase as follows: hematite, arsenopyrite, chalcopyrite, pyrrhotite, and galena (So, 1980 and 1981).

Fig. 18 illustrates the result for present study are in good agreement.

Dependence of Microhardness on Chemical Compositions

Fig. 19 represents the relationship between vickers hardness and Fe content (wt.%) under various test load.

Robertson and Meter (1951) suggested that different contents of iron in the mineral gave a range in hardness: the higher the iron content, the harder the mineral.

As summerized by Vaughan and Craig (1978), several authors have studied the Variation of the hardness of sphalerite (Zn, Fe)S with iron content. All these studies show a sharp increase in hardness on substitution of small amount of iron (<2 wt%) and most studies show a subsequent decrease with iron substitution (>2 wt%).

The microhardness values against the Fe content (wt%) for the studied sphalerite are given in table 8.

In Fig. 19, Vickers hardness of the studied sphalerite is sharpls increased to 8.05 wt% Fe and then

Table 9 Vickers microindentation hardness measured for the oriented sections //(111) and //(100) of the sphalerite and galena.

Examined minerals	Mineral orientation		25gr	50gr	100gr	200gr	300gr	Mean value
Sphalerite	//(111)	m	15.7 15.9	21.6 22.3	30.8 31.2	45.0 45.0	53.5 53.6	
		HV	185.7	191.6	193.0	183.2	193.6	189.4
	//(100)	m	14.5 15.2	21.1 21.4	29.5 30.3	42.4 43.2	52.3 53.2	
		HV	208.8	204.4	207.4	202.5	199.6	204.5
Galena	//(111)	m	24.5 25.0	36.0 36.1	50.0 50.1	69.3 70.5	88.5 90.5	
		HV	75.4	71.1	73.9	75.9	69.5	73.2
	//(111)	m	24.2 25.0	34.8 35.7	48.9 51.0	71.6 73.1	90.1 93.5	
		HV	76.6	74.4	74.2	70.8	66.0	72.4
	//(111)	m	25.0 25.3	35.7 35.8	49.5 49.7	68.0 69.9	82.9 84.5	
		HV	73.0	7.23	75.4	77.9	79.4	75.6
	mean	HV	75.0	72.6	74.5	74.9	71.6	73.7
	//(100)	m	26.3 27.5	36.5 38.5	52.55 53.6	72.0 74.9	92.3 94.5	
		HV	64.1	65.9	65.8	68.7	63.8	65.7
	//(100)	m	25.0 25.7	35.9 37.8	51.2 53.7	75.1 76.2	90.7 92.0	
		HV	71.9	68.1	67.3	64.7	66.6	67.7
	mean	HV	68.0	67.0	66.6	66.7	65.2	66.7
	//(210)	m	25.1 25.3	35.9 36.2	50.0 51.2	73.6 72.4	91.4 94.2	
		HV	73.0	71.1	74.4	69.6	65.0	70.6
Chalcopyrite	//(112)	m	15.3 15.2	22.1 21.4	34.9 34.2	44.9 45.8	58.9 56.6	
		HV	198.0	195.1	154.9	180.0	166.8	178.8

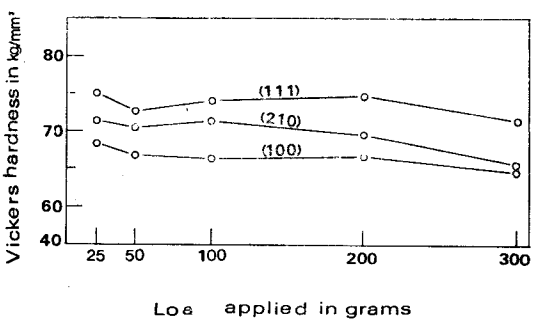

Fig. 21 Vickers microindentation hardness measured for the oriented sections (//(111), //(210) and //(100)) of the galena.

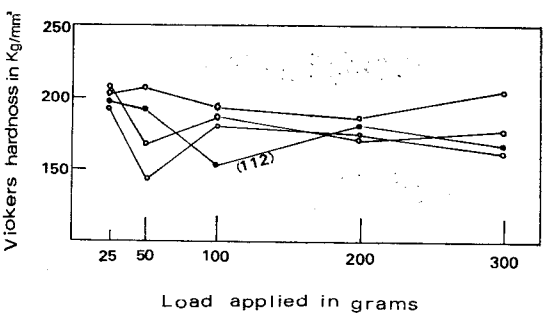

Fig. 22 Variation vickers microindentation hardness for oriented crystal face (//(112)) and unoriented crystal face of Stage I chalcopyrite.

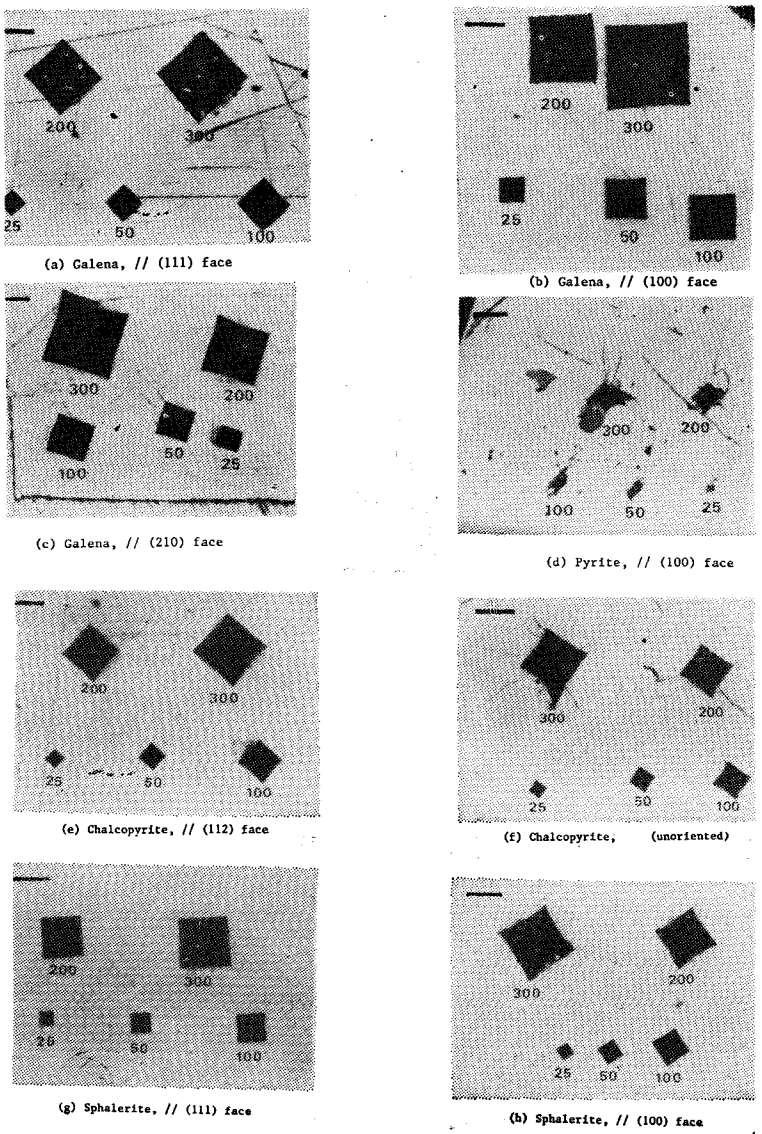

Fig. 23 Photomicrographs of characteristic indentation shapes and fractures of oriented minerals under different test load. bar is 0.1mm.

9). In Fig. 20, Vickers hardness measured on the //(100) polished crystal face is considerably higher than on the //(111) polished crystal face of the studied sphalerite specimen under various load.

For galena specimen, the relationship between hardness values for various face was determined to be $VHN_{(111)} > VHN_{(210)} > VHN_{(100)}$ (Fig. 21). Fig. 22 shows the vickers hardness variation for oriented crystal face (//(112)) and unoriented crystal face of stage II chalcopyrite.

Indentation Shapes and Fracture Characteristics

The indentation shapes and fracture characteristics vary with orientation of the mineral having anisotrophic structures (Young and Millman (1964)), and So (1982 b) have examined the shape and fracture characteristics of identation. Young and Millman (1964) have classified the various shape, deformation and fracture characteristics of indentations: shape characteristics—straight, concave, convex, sigmoidal and fracture characteristics—

Table 10 Characteristics indentation shapes and fractures on oriented mineral surfaces.

	Mineral orientation	Characteristics of Indentation			Characteristics of fracture
		straight	concave	sigmoidal	
Pyrite	//(100)	common	weak		strong radial shells
Chalcopyrite	//(112)	weak	moderte		weak radial
	(unknown)		weak	straight	strong radial
Sphalerite	//(111)	common		weak	
	//(100)		moderate		weak radial
Galena	//(111)	common		weak	
	//(100)		weak	moderate	
	//(210)		weak	straight	

star radial, side radial, cleavage, parting, simple shell, cleavage shell, concentric shell.

Fig. 23 shows the isometric pyrite, galena, sphalerite and tetragonal chalcopyrite exhibit variable indentation shapes and fractures with crystal orientation and are illustrated in table 10.

Pyrite shows common straight or weak concave shapes and simple shell indentation fracture on the unoriented plane, chalcopyrite produced moderate concave shapes and weak side radial fractures on the plane //(112), and strong sigmoidal shapes and strong star radial fractures on the unoriented plane, sphalerite made on common straight or weak sigmoidal shapes on the plane //(111), and moderate concave shapes and weak side radial fractures on the plane //(100), under>100 gram applying loads. Galena shows weak sigmoidal shapes on the plane //(111), moderate sigmoidal shapes on the plane //(100), and strong sigmoidal shapes on the plane //(210), under various load.

Relationship between Reflectance and Vickers hardness Values.

Bowie (1967) produced a useful chart for the identification of ore minerals applying reflectivity–microhardness data measured on the same area. The reflectivities and Vickers microhardness numbers measured for the sulfide ore minerals are mostly plotted within the area closely corresponding to the area of data points made by Bowie (1967) (Fig. 24).

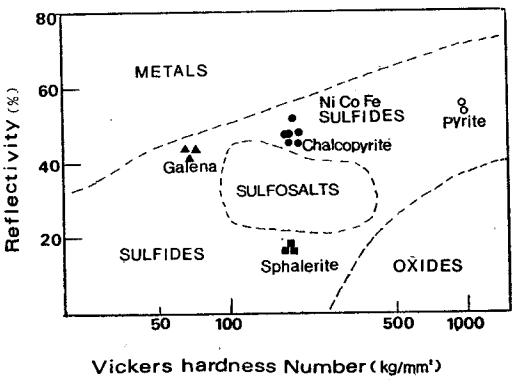

Fig. 24 Reflectivity-microhardness values of the studied minerals plotted on the grouping areas made by Gray and Millman (1962).

ACKNOWLEDGEMENT

The writer express his deepest appreciation to professor Dr. So, C.S. for his continuos guidence and for his intensive participation in this research. Thanks are also due to Mr. Kim, S.H. Seung, Y.H. and Lee, P.K. of Korea university for their help in the beginning of the experimental work.

REFERENCES

Araya, R. A. (1968) Untersuchungen über das Reflexionsvermögen einiger Erzmineralien unter Berücksichtigung unterschiedlicher Versuchsbe dingungen für seine Bestimmung. Ph. D diss. (Mün Chen.), 76p.

Cameron, E. N. (1963) Optical symmetry from reflectivity measurements. Am. Mineral, v. 48, p. 1070—1079.

Cameron E. N. (1966) Ore Microscopy. New York, John Wiley & Sons Inc. Press., 293. p.

Carpenter, R. H. and Bailey, H. C. (1973) Application of Ro and Ar measurements to the study of pyrrhotite and troilite. Am. Mineral. v. 58, p. 440—443

Cervelle, B., Levy, C., and Caye, R. (1971) Dosage rapide du magnesium dans les ilmenites. Mineral. Deposita, v. 6, p. 34—40.

Chang K.H. (1974) Cretaceous stratigraphy of southest Korea. Geol. Soc. Korea Jour., v. 11, p. 1—23.

Chang, T. W., Hwang, S. K., and Lee, D. W. (1983) Geologic Sheet of Chungmu area. 1:50,000.

Charlat, M. and Lèvy, C. (1976) Influence des principales substitutions sur les propriètes optiques dans la série tennantite tétraèdrite. Bull. Soc. Franc. Mineral. Crist. v. 99, p. 29—37.

Eales, H. V. (1967) Reflectivity of gold and gold-silver alloys. Econ. Geol. v. 62, p. 412—420.

Friedman, I., and O'Neil, J. R. (1977) Compilations of stable isotope fractionation factors of geochemical interest. U. S. Geol .Survey Prof. Paper 440 kk, 12 p.

Gray, I. M. and Millman, A. P. (1962) Reflection Characteristics of Ore Minerals. Econ. Geol., v. 57, p. 325—340.

Levy, C. (1967) Contribution a la mineralogie des sulfures de cuivre du type Cu. Mem. Bur. Rech. Geol. Min. No. 54.

Nakhla, F. M. (1956) The hardness of metallic minerals in polished sections. Econ. Geol., v. 51, p. 811—817.

Park, M. E. (1984) Mineralogy, Fluid Inclusion stable isotope and Geochemistry of the Sambo Pb-Zn-Barite Deposits. unpub. Ph. D. Thesis, Korea Univ., 969. p.

Pinet, M., Cervelle, B. and Desnoyers, C. (1978) Reflectance, indice de refraction et expression quantitative de la couleur de proustites et pyragyrites naturelles et artificielles. interpretation genetique. Bull Mineral. v. 101, p. 43—53.

Robertson, F. and Van Meter, W. J. (1951) The Kentron Microhardness Tester, A Quantitative Tool in Opaque Mineral Identification. Econ. Geol., v. 46, p. 541—550.

So, C. S. (1977) Spurenelement-paragenese in Zinkblenden verschiedended Pb-Zn-Vorkommen in Korea. Mineralogical Journal, v. 8, p. 439—455.

SoC. S. and Chi S. J., Shelton, K. L., Skinner, B. (1984) The Copper-Bearing Hydrothermal Vein Deposits in Upper Cretaceous Volcanic Rocks of the Gyeongsang Basin, Republic of Korea. Econ. Geol., v. 79, No. 8.

So, C. S. and Kim, I. K. (1980) Spectral Reflectivity and Microhardness of Some Anisotropic Ore Minerals from Sulfide and Iron Deposits, Korea. Jour. Geol. Soc. Korea, v. 16, No. 1, p. 16—31.

So, C. S. and Jang, Y. N. (1984) Reflection-Microhardness Characteristics and Genesis of Sphalerites from Pb-Zn Deposits in Korea. Jour. Geol. Soc. Korea, v. 20, No. 1, p. 28—40.

So, C. S., Lee, S.M. and Doh, S.J. (1982) Reflection-Microhardness Characteristics and Optical Symmetry of Some Ore Minerals. Jour. Geol. Soc. Korea, v. 18, No. 2, p. 55—66.

So, C. S., and Song, S. H. (1981) Physical Properties of Korean Ore Sulfide Species. Jour. Geol. Soc. Korea, v. 17, No. 1, p. 1—14.

Sourirajan, S., and Kennedy, G. C. (1962) The System H_2O-NaCl at Elevated Temperatures and Pressures. Am. Jour. Sci., v. 260 p. 115—141.

Squair, H. (1965) A Reflectometric Method for Determining the Silver Content of Natural Gold Alloys. Trans. Inst. Min. Metall., v. 74, p. 917—931.

Stanton, R. L. (1972) Ore Petrology. McGraw-Hill Book Company Press., 713p.

Stumpfl. E. F. and Tarkian, M. (1973) Natural Osmium-iridium Alloys and Iron-bearing Platinum. New Electronprobe and Optical Data. Neues Jb. Monat., p. 313—322.

Tarkian, M. (1974) A Key Diagram for the Optical Determination of Common Ore Minerals. Mineral. Sci. Eng., v. 6, p. 101.

Vaughan, D. J. (1978) The Interpretation and Prediction of the Properties of Opaque Minerals from Crystal Chemical Models. Bull. Mineral., v. 101, p. 484—497.

Vaughan, D. J. and Craog, J. R. (1978) Mineral chemistry of Metal Sulfides. Cambridge, England. Cambridge University Press.

Young, B. B. and Millman, A. P. (1964) Microhardness and Deformation Characteristics of Ore Minerals. Trans. Inst. Min. Metall., v. 73, p. 437—466.

三峰銅鑛山産 硫化鑛物의 反射度와 微硬度 特性

池 世 定*

요약 : 본 논문에서는 경남일대 동 광화대에 위치하는 삼봉광산의 함 동—연—아연—은 열수 석영맥을 대상으로 황화 광석광물의 광물학적 특성을 규명하였다. 백악기 경상 퇴적 분지의 상부 지층인 칼크—알카리 화산암류 내에 발달된 N-S~N13°W/65~85°W의 제 단층 열극면 및 압쇄대를 따라 수 개조의 평행한 함 동—연—아연—은 열수 석영맥이 0.5-1.5Km 연장 부존되어 있다. 주 광석광물은 황동석, 방연석, 섬아연석, 황철석 등이며 맥석광물은 석영, 방해석, 견운모, 녹리석 등이다. 이들 광물로 구성된 함 동연—아연—은 석영맥 내에 있어서 부광대의 발달은 구조 규제를 받고 있으며, 수평 및 수직적 방향에 있어서 조성광물의 대상분포 현상을 보여준다. 열수광화작용은 시기적으로 3회에 걸쳐 진행되었다. 광화 제 1 시기(Stage I)는 미량의 황철석과 황동광이 수반하며 제 2 시기에는 황동광, 방연광, 섬아연석과 극미량의 제유화 광물을 수반하는 개발대상의 석영맥(Stage IIa and IIb)이 형성되었고, 제 3 시기에는 이들 석영맥의 약선대를 따라 최후의 방해석맥 (carbonate stage)이 형성되었다.

주조성 광물과 부성분 광물(황동석, 방연석, 섬아연석, 황철석, 유비철석, 백철석, 에나자이트)을 대상으로 물리적 특성을 실험하고, 광물의 형성단계, 부성분, 결정면의 방향과의 상관성을 밝히며 금속광물의 감정을 위한 제 자료를 제시하고자 반사도와 미경도를 실험 연구하였다. 광화시기에 따른 반사력의 특성은 광화작용중 열수계의 물리·화학적 환경의 변화에 따른 광물의 성분 및 구조적 차이에 기인되는 것으로 고려된다. 섬아연석의 반사력과 굴절률은 Zn을 치환하는 철 함량에 정비례하며, //(100) 결정면에서 //(111) 결정면 보다 높은 값을 보여준다. 정성, 정량적인 부성분에 의한 내부반사(백색광하)를 + 니콜하에서만 보여주는 경우 섬아연석은 정상 반사력의 값을 가지나, //니콜하에서도 내부반사를 보이는 것은 매우 상이한 spectral dispersion 을 나타내는데, 내부 반사광과 같은 파장(544mμ, 593mμ, 615mμ)에서 선택반사 효과는 최대가 된다. 불투명 이방성 광석광물인 황동석은 2축성(−)이다.

표준 하중별로 실시한 빅카의 미경도 실험에서, 섬아연석은 100g 하중하에서 철함량이 8.05%에까지 증가함에 따라 미경도 값이 급격히 증가하나 철 성분이 더 많으면 다시 감소하는 경향을 보여준다. 섬아연석은 //(100) 결정면에서 //(111) 결정면보다 미경도 값이 크며, 방연석은 //(111), //(210), //(100)의 순으로 결정방향에 따라 미경도 값이 작아진다. 경도가 작은 유화광물 일수록 indentation의 대각선 길이의 변화폭이 크며, 실험 광물에서는 황철석 섬아연광 황동광 방연광 순으로 증가된다. 한편 모든 실험광물은 결정방향에 따라 각각 특징적인 indentation의 형태와 단구를 갖는데, 이는 광물감정과 결정면의 방향을 규명하는데 좋은 자료가 된다.

*高麗大學校 地質學科